Int. J. Electrochem. Sci., 8 **(2013)** 1885 - 1894

International Journal of
ELECTROCHEMICAL
SCIENCE
www.electrochemsci.org

Structure, Morphology and Electrochemical Properties of $Li[Li_{0.2}Co_{0.4}Mn_{0.4}]O_2$ Cathode Material Synthesized by a Simple Hydrothermal Method

Xin Wei, Shichao Zhang[*]*, Lei He, Guanrao Liu, Puheng Yang*

School of Materials Science and Engineering, Beihang University, Beijing 100191, PR China
[*]E-mail: csc@buaa.edu.cn

Received: 31 December 2012 / *Accepted:* 18 December 2012 / *Published:* 1 February 2013

The nano-sized material $Li[Li_{0.2}Co_{0.4}Mn_{0.4}]O_2$ was synthesized by a simple hydrothermal method. X-ray diffraction results showed that the synthesized material had a hexagonal structure with additional peaks caused by monoclinic distortion. Scanning electron microscopy and transmission electron microscopy showed the homogeneous distribution of particles with 100-200 nm. X-ray photoelectron spectroscopy results indicated that the oxidation states of Co and Mn in $Li[Li_{0.2}Co_{0.4}Mn_{0.4}]O_2$ were present in trivalence and tetravalence, respectively. The charge-discharge curves, cycling performance and d*Q*/d*V* plots were analyzed in detail. The first charge/discharge profile behavior of $Li[Li_{0.2}Co_{0.4}Mn_{0.4}]O_2$ was also discussed. The initial charge and discharge respectively yielded the specific capacity of 199.3 mAh g^{-1} and 174.2 mAh g^{-1}, with relatively high coulombic efficiency of 87.4% at the current density of 100 mA g^{-1} in the voltage range of 2.0-4.6 V at 25 °C.

Keywords: Li-ion battery; Li-rich layered material; Cathode.

1. INTRODUCTION

Up to now, $LiCoO_2$ has been widely applied as one of the cathode materials in commercial lithium-ion batteries due to its good electrochemical performance and its ease of preparation. However, the concerns about high costs, toxicity and structural instability prompted a search for alternative cathode materials [1].

Manganese substitution was considered because it was more abundant and cheaper than Cobalt. Li-rich cathode materials $xLiCoO_2 \cdot (1-x)Li_2MnO_3$ have been studied in the recent past [2-4], mainly due to its high capacity of more than 250 mAh g^{-1} at low rate [5-10]. In these materials, Li_2MnO_3 and Li_2MnO_3-like domains existed with short-range order within a $LiCoO_2$ matrix [9]. Li^+ extraction and oxygen loss from lattice was concurrent at the first charge process of Li-rich layered materials. It

activated a part of Mn^{4+} ions to participate in the following electrochemical reactions, leading to a high discharge capacity [6].

However, the large irreversible capacity loss at the first cycle and inherently low conductivity of the material must be improved prior to its commercial application, which has been the research focus in many scientific groups [9, 11-17]. The large irreversible capacity loss was associated with the oxygen loss from the surface which is further accompanied by the migration of the transition metal ions from the surface to the bulk [12, 15, 16]. Low conductivity was related to the insulating Li_2MnO_3 component, resulting in the poor rate performance [17].

Among the different stoichiometric ratio of xLiCoO$_2$·(1-x)Li$_2$MnO$_3$ compounds, Li[$Li_{0.2}Co_{0.4}Mn_{0.4}$]O$_2$ have been studied by many authors [6, 18-21]. Li[$Li_{0.2}Co_{0.4}Mn_{0.4}$]O$_2$ contained mostly Mn^{4+} in Li_2MnO_3-like atomic environments and Co^{3+} in $LiCoO_2$-like atomic environments, which was intimately mixed over length scales of ≥ 2-3 nm, resulting in a Li[$Li_{0.2}Co_{0.4}Mn_{0.4}$]O$_2$ crystallite composition that appeared homogeneous over the long-range [19]. Various methods have been employed, such as combustion method [22], poly-vinyl alcohol method [20], sol-gel method [21, 23], co-precipitation method [13, 24], and high-temperature solid state method [18, 19]. Nevertheless, few used hydrothermal method to prepare $Li_{1.2}Co_{0.4}Mn_{0.4}O_2$ material to my knowledge.

In this work, we developed a simple hydrothermal method to prepare nano-sized Li[$Li_{0.2}Co_{0.4}Mn_{0.4}$]O$_2$ material. The structure, morphology and electrochemical properties were thoroughly investigated.

2. EXPERIMENTAL

The precursor was prepared by stirring stoichiometric amounts of $Co(CH_3COO)_2$, $Mn(CH_3COO)_2$ and $Li(CH_3COO)$, adding oxalic acid as a precipitating agent and acetic acid as an additive. The suspension was pretreated in a poly(tetrafluoroethylene) (Teflon) container at 150 °C for 3 h. Then the mixture was stirred vigorously until dry. The dried precursor (a) was pressed into pellets and preheated orderly at 450 °C for 4 h (intermediate product: b) and at 500 °C for 3 h (intermediate product: c) in air, and then ground and made into new pellets. After calcining at 750 °C for 3 h in air, the target compound (d) was finally obtained. All the raw materials were analytical purity grade, and the amount of lithium salt was excess in the synthesis.

X-ray diffraction (XRD, Rigaku D/Max-2400, Japan) using Cu Kα radiation was used to identify the crystalline phase of the synthesized materials. The data were collected in the 2θ range of 10-80° and the patterns were refined by the Rietveld method with the General Structure Analysis Software (GSAS program). Scanning electron microscopy (SEM, Hitachi S-4800, Japan), transmission electron microscopy (TEM) were engaged in observing morphology, size and distribution of as-prepared materials. X-ray photoelectron spectroscopy (XPS) was obtained using American PHI5700ESCA with monochromatic Al Kα radiation, the chemical valence state of the transition metal elements was determined. Binding energy was corrected using C 1s peak (285.0 eV).

The electrode was fabricated by coating a slurry of 75 wt.% active materials, 15 wt.% carbon black, and 10 wt.% poly(vinylidene fluoride) (PVDF) binder dissolved in N-methyl pyrrolidone

(NMP) onto an aluminum foil substrate. Subsequently, the electrode was dried at 100 °C for 2h under vacuum. The film was cut into pieces of about 0.8×0.8 cm^2 to act as cathode. The testing half-cells were assembled in an argon-filled glove box (MB-10-G with TP170b/mono, MBRAUN) with lithium metal as counter and reference electrode. Electrolyte was 1 M $LiPF_6$ in a mixed solution of EC and DMC (1:1 in volume ratio). The charge-discharge measurements were galvanostatically carried out by using a battery test system (NWEARE BTS-610, Neware Technology Co., Ltd., China) at different current density (100 mA g^{-1}, 200 mA g^{-1} and 400 mA g^{-1}) in the voltage range of 2.0-4.6 V (vs. Li/Li^+) at 25°C.

3. RESULTS AND DISCUSSION

Fig. 1 shows X-ray diffraction patterns of the precursors (a), intermediate product (b and c), and $Li[Li_{0.2}Co_{0.4}Mn_{0.4}]O_2$ sample (d). The precursor (Fig. 1a) consists of MnC_2O_4 (indexed PDF No. 25-544, monoclinic, Space Group: C2/c) and CoC_2O_4 (indexed PDF No. 25-250, orthorhombic, Space Group: Cccm). As shown in Fig. 1d, most of the diffraction peaks can be indexed to the α-$NaFeO_2$ structure with space group of $R\bar{3}m$. The weak reflections with 20-25° are originated from the monoclinic Li_2MnO_3-like (C2/m) super lattice, which corresponds to the ordering of the Li^+ and Mn^{4+} ions in the transition metal layer [25]. Compared to Fig. 1d, impurity phase can be found after preheating at 450 °C (Fig. 1b). After preheating at 500 °C (Fig. 1c), no impurity phase can be detected. However, there are no splitting of both (006)/(012) and (018)/(110), indicating that the desired layered structure does not exist. Finally when calcined at 750 °C (Fig. 1d), no impurity phase exists. The pronounced splitting of both (006)/(012) and (018)/(110) can be observed, suggesting fine layered structure.

The synthesis procedures are expressed as follows:

$$Co^{2+} + Mn^{2+} + 2C_2O_4^{2-} \rightarrow CoC_2O_4 \downarrow + MnC_2O_4 \downarrow \quad (1)$$

$$2CoC_2O_4 + 2MnC_2O_4 + 6Li^+ + 5O_2 \rightarrow 5Li_{1.2}Co_{0.4}Mn_{0.4}O_2 + 8CO_2 \quad (2)$$

Fig. 2 shows the Rietveld refined results for the XRD pattern of $Li[Li_{0.2}Co_{0.4}Mn_{0.4}]O_2$ material. Due to the complexity of the $xLi_2MnO_3 \cdot (1-x)LMO_2$ structures, the prototypic $R\bar{3}m$ symmetry of layered $LiMO_2$ compounds is used for the refinement [9, 24]. The Li^+ ions occupy the 3b (0, 0, 0.5) site (1.0 mol) and 3a (0, 0, 0) site (0.2 mol). The Co^{3+} and Mn^{4+} ions are located at 3a (0, 0, 0) site, and the O^{2-} ions are located at the 6c (0, 0, 0.2588) site [23]. The 3a/3b cation mixing is negligible because the radius of Co^{3+} (0.545 Å) and Mn^{4+} (0.53 Å) are much smaller than that of Li^+ (0.76 Å). The hexagonal lattice parameter is refined to be a = 2.828(3) Å, c = 14.149(6) Å.

Fig. 3 shows SEM, TEM and EDX images of precursors (a), intermediate products (b and c) and $Li[Li_{0.2}Co_{0.4}Mn_{0.4}]O_2$ sample (d). The micro-robs with the width of 400-600 nm and the length of 1-2 μm can be seen, as shown in Fig. 3a.

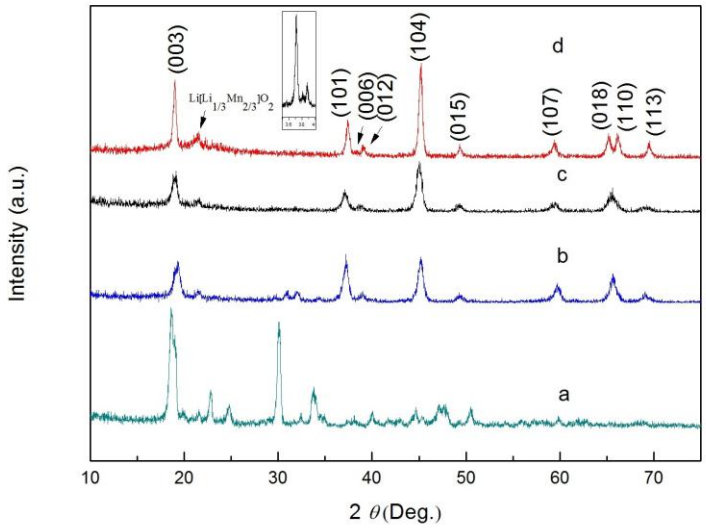

Figure 1. XRD patterns of the precursors (a), intermediate product (b and c), and $Li[Li_{0.2}Co_{0.4}Mn_{0.4}]O_2$ sample (d).

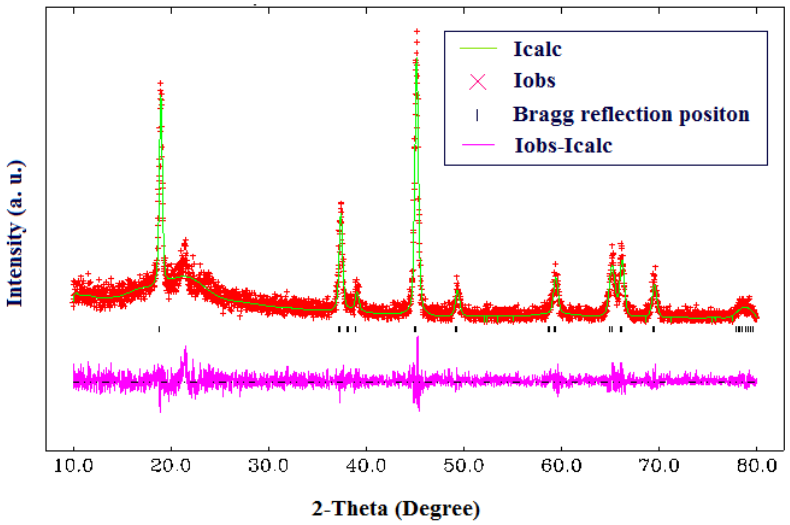

Figure 2. Rietveld refined results for the XRD pattern of $Li[Li_{0.2}Co_{0.4}Mn_{0.4}]O_2$ material.

Through two-step preheated, micro-robs are gradually split up into pieces and grains (Fig. 3b and 3c). After final calcining, the as-prepared $Li[Li_{0.2}Co_{0.4}Mn_{0.4}]O_2$ (Fig. 3d) exhibits the nano-sized gains with the range of 100-200 nm. From the data of EDX tests, atomic ratio of Co, Mn, O in $Li[Li_{0.2}Co_{0.4}Mn_{0.4}]O_2$ sample (d) are respectively 14.18%, 10.51%, and 75.30%, close to the stoichiometric ratio of raw materials. Fig. 4 shows Co2*p* and Mn2*p* XPS spectra of $Li[Li_{0.2}Co_{0.4}Mn_{0.4}]O_2$ material. The sharp peaks Co2$p_{3/2}$ and Co2$p_{1/2}$ are at 779.9 eV and 794.9 eV, and two satellite peaks are respectively at 789.5 eV and 804.6 eV in the Co2*p* spectra.

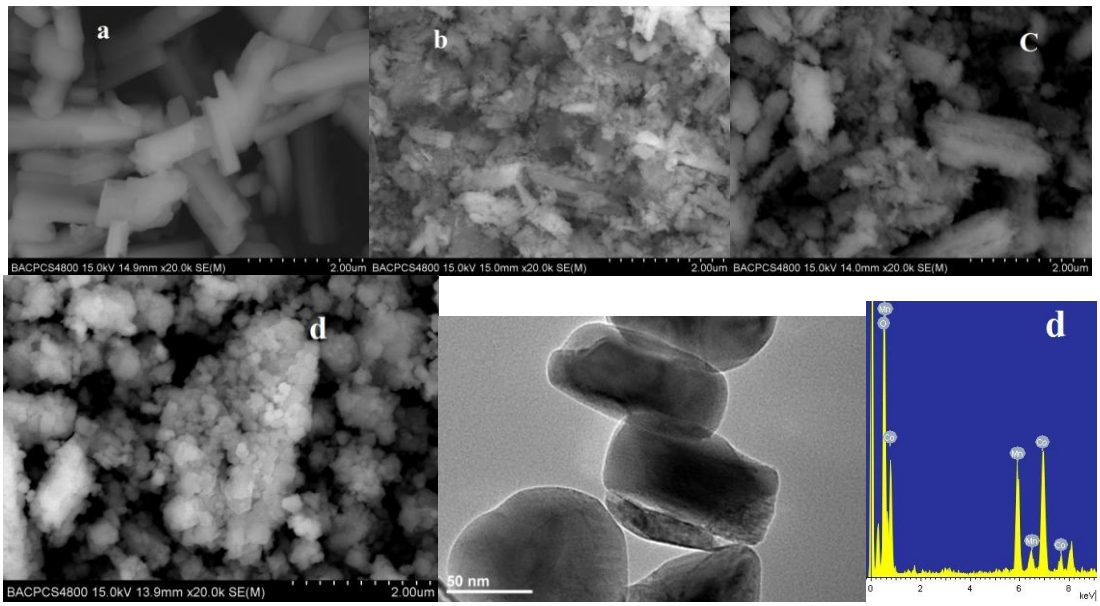

Figure 3. SEM images for the precursors a (a), intermediate product (b and c), and $Li[Li_{0.2}Co_{0.4}Mn_{0.4}]O_2$ sample (d)； TEM image for $Li[Li_{0.2}Co_{0.4}Mn_{0.4}]O_2$ sample (d); EDX images for $Li[Li_{0.2}Co_{0.4}Mn_{0.4}]O_2$ sample (d) .

This value matches well with the BE reported for Co^{3+} ($Co2p_{3/2}$, 780.1 eV and 790.0 eV) in the previous work [23].

In the Mn*2p* spectra, the major peak $Mn2p_{3/2}$ is at 642.2 eV and the minor one $Mn2p_{1/2}$ is at 653.8 eV. The BE for $Mn2p_{3/2}$ spectra is in good agreement with the value reported for Mn^{4+} (642.4 eV) [23]. The present XPS results indicate that the oxidation states of Co and Mn in $Li[Li_{0.2}Co_{0.4}Mn_{0.4}]O_2$ are present in trivalence and tetravalence, respectively.

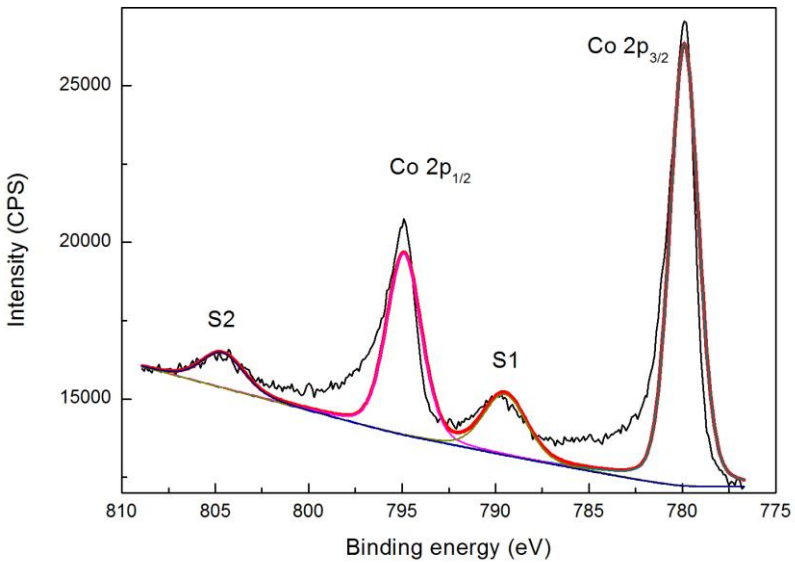

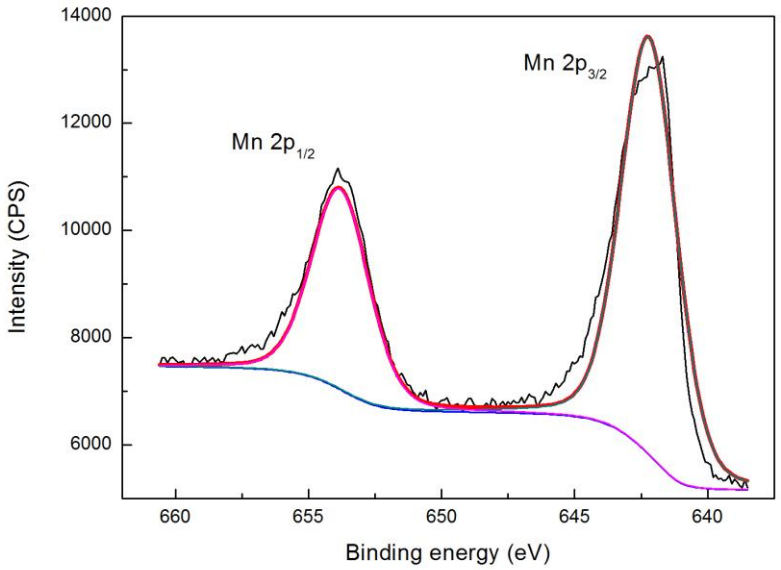

Figure 4. Co2*p* and Mn2*p* XPS spectra of $Li[Li_{0.2}Co_{0.4}Mn_{0.4}]O_2$ material.

Fig. 5 shows the charge-discharge profiles of $Li[Li_{0.2}Co_{0.4}Mn_{0.4}]O_2$ at 100 mAh g^{-1}. The initial charge and discharge cycle yields specific capacity of 199.3 mAh g^{-1} and 174.2 mAh g^{-1}, with the coulombic efficiency of 87.4%. The slope region (3.4-4.4 V) of the initial charge is attributed to the extraction of Li^+ from the lithium layer (80.3 mAh g^{-1}), associated with the oxidation of Co^{3+} to Co^{4+} [26]. The following long plateau (4.4-4.6 V) is due to lithium extraction and oxygen loss (119.0 mAh g^{-1}) [15, 27], which is absent during the subsequent charge. It is consistent with the irreversible removal of Li_2O from the Li_2MnO_3 component [6].

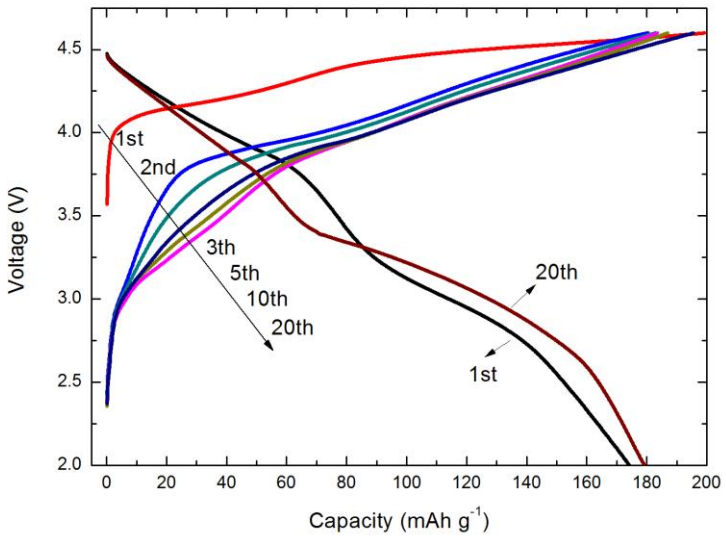

Figure 5. The charge-discharge curves of prepared $Li[Li_{0.2}Co_{0.4}Mn_{0.4}]O_2$ sample at a current density of 100 mAh g^{-1}.

Fig. 6 shows d*Q*/d*V* plots of the synthesized $Li[Li_{0.2}Co_{0.4}Mn_{0.4}]O_2$ sample. As shown in Fig. 6a, during the first cycle, the first anodic peak (~4.17 V) corresponds to lithium extraction and simultaneous oxidation of Co^{3+}. The next peak at ~4.46 V is the result from the irreversible removal of Li_2O from the Li_2MnO_3 component and the formation of electrochemical active MnO_2 component. The peak (~4.46 V) disappears during the subsequent cycles, confirming its irreversibility. During the following cycles, the main anodic peak shifts from 4.17 V to 3.94 V, indicating that the structure and/or the electrode/electrolyte interface may have been modified after the first cycle. The peaks at around 3.94 V are related to the oxidation of Co^{3+} and Mn^{3+}. As reported by Deng et al. [31], the oxidation of Mn^{3+} ions made a small contribution to the capacity at around 4.0 V. At 10th and 20th cycles, abroad anodic peak corresponding to the extraction of lithium ions occurred at 3.94 V (main peak) and 4.28 V (secondary peak, more pronounced than 2nd cycle).

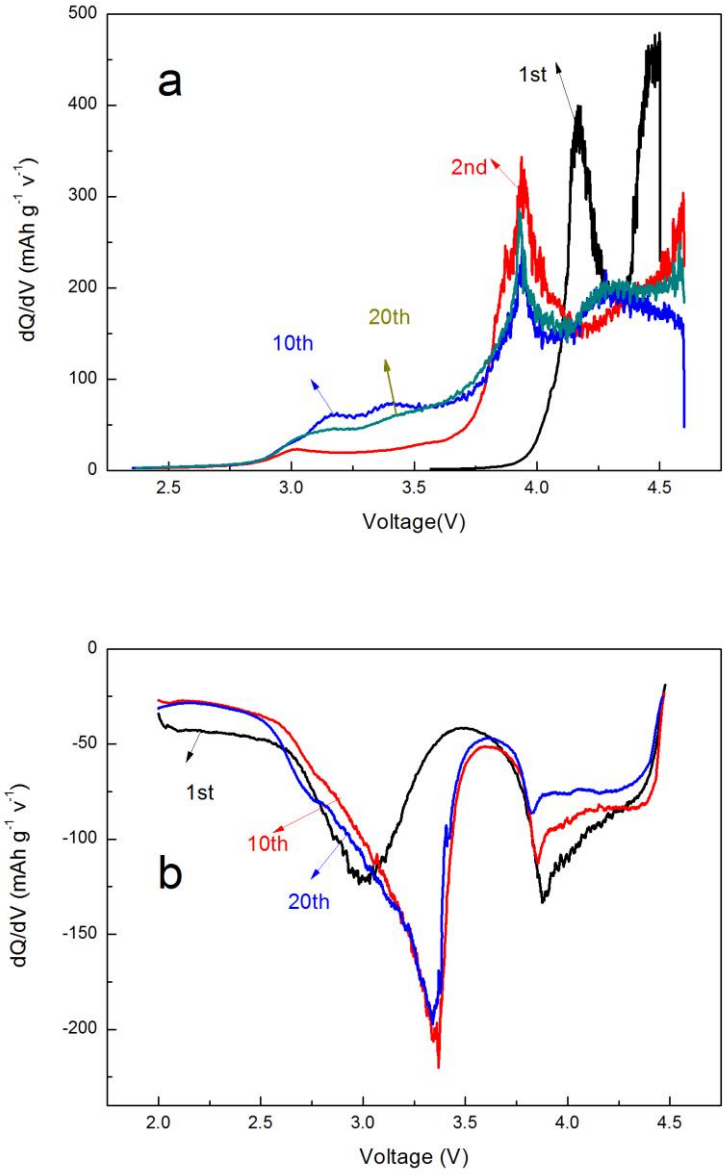

Figure 6. d*Q*/d*V* plots of the synthesized $Li[Li_{0.2}Co_{0.4}Mn_{0.4}]O_2$ sample.

In Fig. 6b, during the initial discharge, the cathodic peaks at 3.88 V and 3.00 V can be observed, which corresponds with lithium insertion and reduction of Co^{4+}. It has been reported that these two peaks may be associated with lithium occupation of tetrahedral and octahedral sites [28-30]. A weak cathodic peak (~2.75 V in the 10th and 20th cycles) is probably to be related to the partial reduction of Mn^{4+} to Mn^{3+} ions [9, 31].

Fig. 7 shows the cycling performance of the materials at different current densities of 100, 200 and 400 mA g^{-1}. The material has an initial discharge capacity of 174.2 mAh g^{-1} when cycling at 100 mA g^{-1}. The discharge capacity gradually increases to 190.8 mAh g^{-1} at the 5th cycle and then decreases to 185.7 mAh g^{-1} at the 10th cycle. It subsequently ascends to 194.3 mAh g^{-1} at the 13th cycle and descends to 160.0 mAh g^{-1} after 40 cycles. When the current density rises to 200 mA g^{-1}, the initial discharge capacity is 141.5 mAh g^{-1}, which increases to 164.3 mAh g^{-1} at the 7th cycle and reduces to 134.3 mAh g^{-1} after 40 cycles. When the current density rises to 400 mA g^{-1}, the initial discharge capacity is 130.5 mAh g^{-1} and gradually ascends to 144.6 mAh g^{-1} at the 3th cycle, subsequently descending to 92.1 mAh g^{-1} after 40 cycles. The capacity retentions are respectively 91.8%, 94.9% and 70.6% at the current density of 100, 200 and 400 mA g^{-1}. The cells endure an activation process where the capacity gradually increases in the first several cycles. With the increasing of cycle number, the material transforms to a spinel-like phase [22]. This phase transformation is believed to be induced by the Jahn-Teller of active Mn^{3+} ions. It is proposed that the gradual capacity decay is a result of transition-metal-ions solubility induced by the well-known disproportion reaction: $2Mn^{3+} \rightarrow Mn^{4+} + Mn^{2+}$ that occurs as a result of the high concentration of Mn^{3+}. Therefore, the gradual capacity decay is partly attributed to this structural instability during charge-discharge cycling.

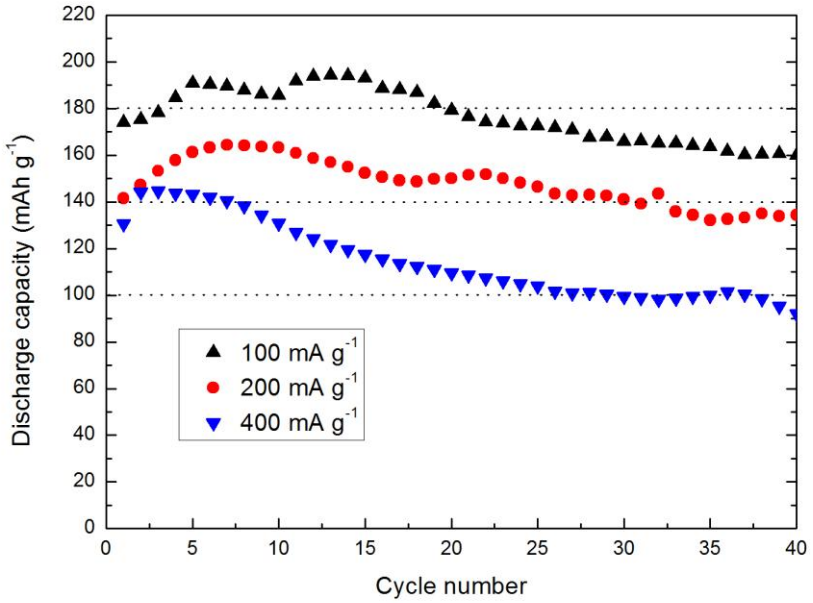

Figure 7. Galvanostatic cycling performance of the $Li[Li_{0.2}Co_{0.4}Mn_{0.4}]O_2$ sample.

4. CONCLUSIONS

The nano-sized $Li[Li_{0.2}Co_{0.4}Mn_{0.4}]O_2$ particles was synthesized via a simple hydrothermal method. Structure and electrochemical properties were thoroughly investigated. Nanomaterial provided short diffusion length and more active surface area for Li intercalation. It exhibited relatively high coulombic efficiency of 87.4% of the first cycle when cycling at 100 mA g^{-1}. The capacity retentions were respectively 91.8%, 94.9% and 70.6% at the current density of 100, 200 and 400 mA g^{-1}. High rate performance yet has to be improved. Much work needs to be done in order to meet its commercial application.

ACKNOWLEDGEMENTS
This work was supported by the National Basic Research Program of China (973 Program) (2013CB934001), National Natural Science Foundation of China (51074011 and 51274017) and National 863 Program (2007AA03Z231 and 2011AA11A257).

References

1. H. Li, Z.X. Wang, L.Q. Chen, X.J. Huang, *Adv. Mater.* 21 (2009) (45) 4593.
2. T.A. Arinkumar, Y. Wu, A. Manthiram, *Chem. Mater.* 19 (2007) (12) 3067.
3. Y. Wu, A. Manthiram, *Solid State Ionics* 180 (2009) (1) 50.
4. G. Singh, W.C. West, J. Soler, R.S. Katiyar, *J. Power Sources* 218 (2012) 34.
5. M.M. Thackeray, C.S. Johnson, J.T. Vaughey, N. Li, S.A. Hackney, *J. Mater. Chem.* 15 (2005) (23) 2257.
6. M.M. Thackeray, S.H. Kang, C.S. Johnson, J.T. Vaughey, R. Benedek, S.A. Hackney, *J. Mater. Chem.*17 (2007) (30) 3112.
7. A. Ito, D.C. Li, Y. Sato, M. Arao, M. Watanabe, M. Hatano, H. Horie, Y. Ohsawa, *J. Power Sources* 195 (2010) (2) 567.
8. J.H. Lim, H. Bang, K.S. Lee, K. Amine, Y.K. Sun, *J. Power Sources* 189 (2009) (1) 571.
9. S.H. Kang, C.S. Johnson, J.T. Vaughey, K. Amine, M.M. Thackeray, *J. Electrochem. Soc.* 153 (2006) (6) A1186.
10. J.M. Zheng, Z.R. Zhang, X.B. Wu, Z.X. Dong, Z. Zhu, Y. Yang, *J. Electrochem. Soc.*155 (2008) (10) A775.
11. Z.Q. Deng, A. Manthiram, *J. Phys. Chem. C* 115 (2011) (14) 7097.
12. W.C. West, R.J. Staniewicz, C. Ma, J. Robak, J. Soler, M.C. Smart, B.V. Ratnakumar, *J. Power Sources* 196 (2011) (22) 9696.
13. N. Yabuuchi, K. Yoshii, S.T. Myung, I. Nakai, S. Komaba, *Journal of the American Chemical Society* 133 (2011) (12) 4404.
14. J. Gao, J. Kim, A. Manthiram, *Electrochem. Commun.* 11 (2009) (1) 84.
15. A.R. Armstrong, M. Holzapfel, P. Novak, C.S. Johnson, S.H. Kang, M.M. Thackeray, P.G. Bruce, *Journal of the American Chemical Society* 128 (2006) (26) 8694.
16. N. Tran, L. Croguennec, M. Menetrier, F. Weill, P. Biensan, C. Jordy, C. Delmas, *Chem. Mater* 20 (2008) (15) 4815.
17. S.H. Kang, P. Kempgens, S. Greenbaum, A.J. Kropf, K. Amine, M.M. Thackeray, *J. Mater. Chem.* 17 (2007) (20) 2069.
18. J.G. Wen, J. Bareno, C.H. Lei, S.H. Kang, M. Balasubramanian, I. Petrov, D.P. Abraham, *Solid State Ionics* 182 (2011) (1) 98.

19. J. Bareno, M. Balasubramanian, S.H. Kang, J.G. Wen, C.H. Lei, S.V. Pol, I. Petrov, D.P. Abraham, *Chem. Mater* 23 (2011) (8) 2039.
20. J.-M. Kim, S. Tsuruta, N. Kumagai, *Electrochem. Commun.* 9 (2007) (1) 103.
21. Z. Li, Y. Wang, X. Bie, K. Zhu, C. Wang, G. Chen, Y. Wei, *Electrochem. Commun.* 13 (2011) (9) 1016.
22. Y.J. Park, Y.S. Hong, X.L. Wu, M.G. Kim, K.S. Ryu, S.H. Chang, *J. Electrochem. Soc.*151 (2004) (5) A720.
23. Y.J. Wei, K. Nikolowski, S.Y. Zhan, H. Ehrenberg, S. Oswald, G. Chen, C.Z. Wang, H. Chen, *Electrochem. Commun.*11 (2009) (10) 2008.
24. J. Zheng, S.N. Deng, Z.C. Shi, H.J. Xu, H. Xu, Y.F. Deng, Z. Zhang, G.H. Chen, *J. Power Sources* 221 (2013) 108.
25. D.Y.W. Yu, K. Yanagida, H. Nakamura, *J. Electrochem. Soc.*157 (2010) (11) A1177.
26. X.-J. Guo, Y.-X. Li, M. Zheng, J.-M. Zheng, J. Li, Z.-L. Gong, Y. Yang, *J. Power Sources* 184 (2008) (2) 414.
27. Z.H. Lu, L.Y. Beaulieu, R.A. Donaberger, C.L. Thomas, J.R. Dahn, *J. Electrochem. Soc.*149 (2002) (6) A778.
28. C.S. Johnson, N. Li, C. Lefief, J.T. Vaughey, M.M. Thackeray, *Chem. Mater* 20 (2008) (19) 6095.
29. J. Breger, Y.S. Meng, Y. Hinuma, S. Kumar, K. Kang, Y. Shao-Horn, G. Ceder, C.P. Grey, *Chem. Mater* 18 (2006) (20) 4768.
30. H.H. Li, N. Yabuuchi, Y.S. Meng, S. Kumar, J. Breger, C.P. Grey, Y. Shao-Horn, *Chem. Mater.* 19 (2007) (10) 2551.
31. H.X. Deng, I. Belharouak, Y.K. Sun, K. Amine, *J. Mater. Chem.*19 (2009) (26) 4510.